Provided for non-commercial research and education use.
Not for reproduction, distribution or commercial use.

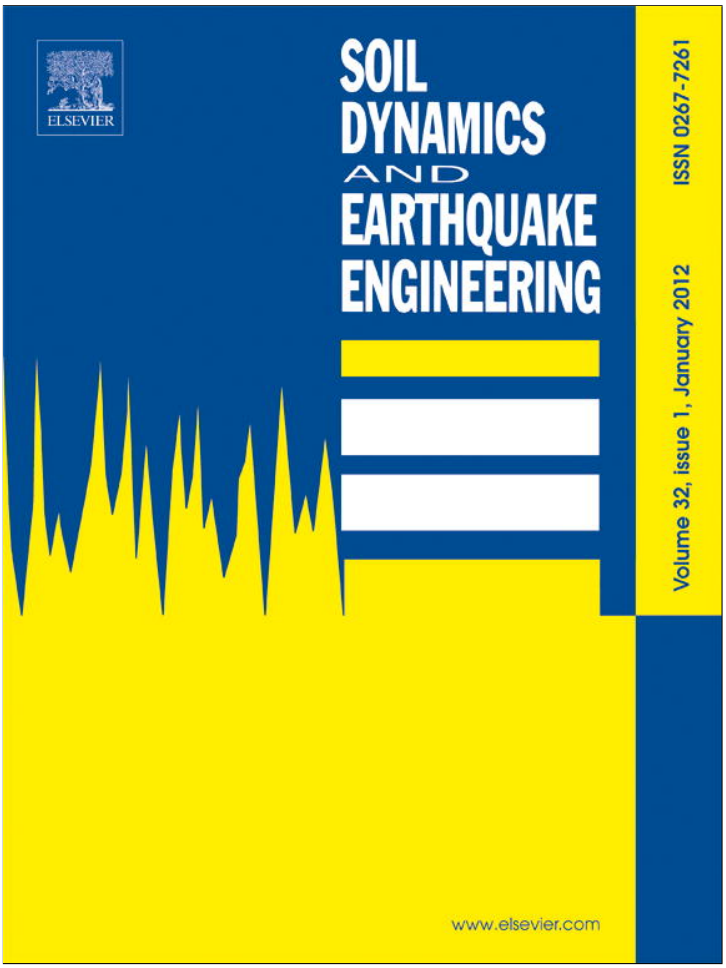

(This is a sample cover image for this issue. The actual cover is not yet available at this time.)

This article appeared in a journal published by Elsevier. The attached copy is furnished to the author for internal non-commercial research and education use, including for instruction at the authors institution and sharing with colleagues.

Other uses, including reproduction and distribution, or selling or licensing copies, or posting to personal, institutional or third party websites are prohibited.

In most cases authors are permitted to post their version of the article (e.g. in Word or Tex form) to their personal website or institutional repository. Authors requiring further information regarding Elsevier's archiving and manuscript policies are encouraged to visit:

http://www.elsevier.com/copyright

Author's personal copy

Soil Dynamics and Earthquake Engineering 49 (2013) 135–145

Contents lists available at SciVerse ScienceDirect

Soil Dynamics and Earthquake Engineering

journal homepage: www.elsevier.com/locate/soildyn

Direct differentiation method for response sensitivity analysis of a bounding surface plasticity soil model

Quan Gu [a], Gang Wang [b,*]

[a] School of Architecture and Civil Engineering, Xiamen University, Xiamen, Fujian 361005, PR China
[b] Department of Civil and Environmental Engineering, Hong Kong University of Science and Technology, Clear Water Bay, Kowloon, Hong Kong

ARTICLE INFO

Article history:
Received 17 February 2012
Received in revised form
26 January 2013
Accepted 31 January 2013

ABSTRACT

Finite element (FE) response sensitivity analysis is an important component in gradient-based structural optimization, reliability analysis, system identification, and FE model updating. In this paper, the FE response sensitivity analysis methodology based on the direct differentiation method (DDM) is applied to a bounding surface plasticity material model that has been widely used to simulate nonlinear soil behavior under static and dynamic loading conditions. The DDM-based algorithm is derived and implemented in the general-purpose nonlinear finite element analysis program OpenSees. The algorithm is validated through simulation of the nonlinear cyclic response of a soil element and a liquefiable soil site at Port Island, Japan, under earthquake loading. The response sensitivity results are compared and validated with those obtained from Forward Finite Difference (FFD) analysis. Furthermore, the results are used to determine the relative importance of various soil constitutive parameters to the dynamic response of the system. The DDM-based algorithm is demonstrated to be accurate and efficient in computing the FE response sensitivities, and has great potential in the sensitivity analysis of nonlinear dynamic soil-structure systems.

© 2013 Published by Elsevier Ltd.

1. Introduction

Finite element (FE) response sensitivity analysis is an essential ingredient of gradient-based optimization methods and is required in structural optimization, system identification, reliability, and FE model updating [1–4]. Furthermore, the sensitivity analysis results may be used to propagate the material and loading uncertainty to the structural responses of interest. In addition, FE response sensitivities provide invaluable insight into the effects of system parameters on, and their relative importance to, the system response [5]. Several methods are available for response sensitivity analysis, including the Finite Difference Method (FDM), the Adjoint Method (AM), the Perturbation Method (PM), and the Direct Differentiation Method (DDM) [6–11]. The FDM is the simplest method for response sensitivity computation, but is computationally expensive and can be negatively affected by numerical noise. The AM is efficient for linear and non-linear elastic systems, but is not a competitive method for path-dependent (i.e., inelastic) problems. The PM is computationally efficient but generally not very accurate. The DDM, on the other hand, is a general, accurate and efficient method that is applicable to any material constitutive model. The DDM-based response sensitivity analysis methodology shows great promise in the analysis of large and complex structural or geotechnical systems.

However the DDM method requires analytical derivations and their computer implementation to differentiate the system responses with respect to sensitivity parameters. Over the past decade, the DDM-based sensitivity analysis method has been actively developed and implemented in an open source FE analysis framework known as OpenSees [12]. The DDM has been developed for various constitutive models including uniaxial materials, three-dimensional J_2 plasticity models and pressure-independent multi-yield surface J_2 plasticity models [13]. These models can be used to simulate truss and beam components in structures, and nonlinear clay behaviors. Detailed descriptions of the DDM-based sensitivity analysis methodology implemented in OpenSees can be found in the literature [14–17].

Yet, the method has not been formulated for sandy soils, which usually exhibit different behavior from clayey soils, such as pressure-dependent cyclic behaviors, shear-induced volumetric dilation and contraction, as well as liquefaction under low effective confinement. The objective of this paper is to extend the DDM-based sensitivity analysis to a class of bounding surface models for sandy soils. The bounding surface model has been widely used and proven to be an effective and robust model to simulate the behaviors of sandy materials under cyclic and seismic loading conditions [18–21]. The DDM-based sensitivity algorithm is particularly

* Corresponding author. Tel.: +852 2358 7161; fax: +852 2358 1534.
E-mail address: gwang@ust.hk (G. Wang).

0267-7261/$ - see front matter © 2013 Published by Elsevier Ltd.
http://dx.doi.org/10.1016/j.soildyn.2013.01.028

Author's personal copy

efficient for strongly nonlinear, large-scale problems with a large number of sensitivity parameters. Geotechnical problems modeled using the bounding surface model are such examples. Thus developing a DDM-based sensitivity algorithm for the bounding surface model will allow us to solve a large number of challenging geotechnical problems, such as the earthquake-induced liquefaction phenomenon in sandy soils. When combined with the existing sensitivity analysis framework for clayey soils and soil-structure systems, the DDM-based sensitivity analysis may be readily applied to real soil-foundation-structure interaction systems [17].

This paper provides a summary of the bounding surface model and detailed DDM formulation, followed by examples to validate the DDM-based FE response sensitivity algorithm. The algorithm is applied to study the sensitivity of liquefied ground responses observed at Port Island in Japan under a real earthquake scenario. The results are further used to identify the relative importance of the soil parameters to the ground surface response.

2. Numerical implementation of a bounding surface model

The bounding surface model presented herein was developed for simulating the pressure-dependent behaviors of sandy soils under complex loading conditions [18,19]. Compared with the classical plastic theory using yield surfaces, flow rules and hardening laws to characterize the plastic behavior of a material, this model generalizes the yield-surface-based plasticity theory by defining a bounding surface or a failure surface. The plastic deformation within the bounding surface is determined by a varying plastic modulus, which is defined as a continuous function of the distance from the current stress to a properly defined 'image' stress on the bounding surface. The model was further improved to incorporate the basic premises of critical-state soil mechanisms to allow for the realistic modeling of the shear-induced volumetric changes (i.e., contraction or dilation) in either a loose or a dense state, and the phase transition from one state to another [20,21], which is the basis for modeling the liquefaction behavior of sandy soils. In practice, this model has been implemented in some commercial softwares, and verified using extensive experimental data and real earthquake records [22].

2.1. Constitutive formulation

The bounding surface model employs a stress ratio invariant, defined as $R=\left(\frac{1}{2}\mathbf{r}:\mathbf{r}\right)^{1/2}$, where $\mathbf{r}$ is the stress ratio of the deviatoric stress $\mathbf{s}$ over pressure p, i.e., $\mathbf{r}=\frac{\mathbf{s}}{p}$, and the notation ":" is the double contraction between two second-order tensors, i.e., $\mathbf{A}:\mathbf{B}=A_{ij}B_{ij}$. Accordingly, an ultimate failure surface, or a failure-bounding surface, is defined as

$$\hat{f}=R-R_f=0 \tag{1}$$

where the parameter R_f is the stress ratio invariant at the failure surface, which is related to the corresponding classical critical state triaxial parameter M by $R_f=M/\sqrt{3}$. Stress is not allowed to trespass the failure-bounding surface $\hat{f}=0$. Similarly, the maximum prestress memory bounding surface is defined as:

$$\bar{f}=R-R_m=0 \tag{2}$$

where R_m is a history parameter providing the maximum prestress level. The two bounding surfaces $\hat{f}=0$ and $\bar{f}=0$ are combined to compute the plastic modulus.

Inside the failure-bounding surface, the hypoelastic response, i.e., the elastic strain rate $\dot{\boldsymbol{\varepsilon}}^e$, is defined as the summation of deviatoric strain $\dot{\mathbf{e}}^e$ and volumetric strain $tr\dot{\boldsymbol{\varepsilon}}^e$:

$$\dot{\boldsymbol{\varepsilon}}^e=\dot{\mathbf{e}}^e+\frac{1}{3}(tr\dot{\boldsymbol{\varepsilon}}^e)\mathbf{I}=\frac{1}{2G}\dot{\mathbf{s}}+\frac{1}{3K}\dot{p}\mathbf{I}=\frac{1}{2G}p\dot{\mathbf{r}}+\left(\frac{1}{2G}\mathbf{r}+\frac{1}{3K}\mathbf{I}\right)\dot{p} \tag{3}$$

where G and K are the pressure-dependent elastic shear and bulk moduli, respectively. Similarly, the hypoplastic response, i.e., the plastic strain rate $\dot{\boldsymbol{\varepsilon}}^p$, can be written as

$$\dot{\boldsymbol{\varepsilon}}^p=\left(\frac{1}{H_r}\mathbf{n}_D+\frac{1}{3K_r}\mathbf{I}\right)(p\dot{\mathbf{r}}:\mathbf{n}_N)+\left(\frac{1}{H_p}\mathbf{r}+\frac{1}{3K_p}\mathbf{I}\right)h(p-p_m)\langle\dot{p}\rangle \tag{4}$$

where H_r and K_r are, respectively, the plastic shear and bulk moduli associated with the deviatoric stress ratio $\dot{\mathbf{r}}$; parameters H_p and K_p are, respectively, the plastic shear and bulk moduli associated with the pressure rate $\dot{p}$. The vectors $\boldsymbol{n}_D$ and $\boldsymbol{n}_N$ are unit vectors in stress space along the deviatoric part of $\dot{\boldsymbol{\varepsilon}}^p$ and the associated deviatoric loading direction, respectively. In this paper both $\boldsymbol{n}_D$ and $\boldsymbol{n}_N$ are taken to be the same as the unit vector normal to the maximum prestress memory bounding surface $\bar{f}=0$ (i.e., vector $\mathbf{n}$ in Fig. 1). The p_m is the maximum value of mean pressure p experienced in past loading. The Heaviside step function $h(p-p_m)$ and the Macaulay brackets $\langle\,\rangle$ around $\dot{p}$ indicate that the plastic mechanism due to $\dot{p}$ operates only when $p=p_m$ and $\dot{p}>0$. As shown in Fig. 1, the previous unloading stress point (i.e., $\boldsymbol{\alpha}$ in Fig. 1), the current deviatoric stress ratio $\mathbf{r}$ and a properly defined 'image' stress $\bar{\mathbf{r}}$ on the maximum prestress memory bounding surface $\bar{f}(\boldsymbol{\sigma})=0$ are combined to determine variable plastic moduli H_r and Kr, which are continuous functions of the distance ρ from $\boldsymbol{\alpha}$ to $\mathbf{r}$ ($\rho=\|\mathbf{r}-\boldsymbol{\alpha}\|_2$) and the distance $\bar{\rho}$ from $\boldsymbol{\alpha}$ to $\bar{\mathbf{r}}$ ($\bar{\rho}=\|\bar{\mathbf{r}}-\boldsymbol{\alpha}\|_2$) [18]. It is worth mentioning that for practical applications, the shear-induced plastic strains usually dominate. Therefore, the second term in Eq. (4), i.e., $\left(\frac{1}{H_p}\mathbf{r}+\frac{1}{3K_p}\mathbf{I}\right)h(p-p_m)\langle\dot{p}\rangle$, is neglected in this paper for simplicity. The plastic strain rate $\dot{\boldsymbol{\varepsilon}}^p$ can be simplified as:

$$\dot{\boldsymbol{\varepsilon}}^p=\left(\frac{1}{H_r}\mathbf{n}+\frac{1}{3K_r}\mathbf{I}\right)(p\dot{\mathbf{r}}:\mathbf{n}) \tag{5}$$

2.2. Numerical implementation

The numerical implementation of the constitutive model employs an explicit algorithm for computing the plastic moduli H_r and K_r. In this section, the discretized version of the constitutive model is presented in detail. The variables with subscript n denote the ones at the last time step at discrete time t_n.

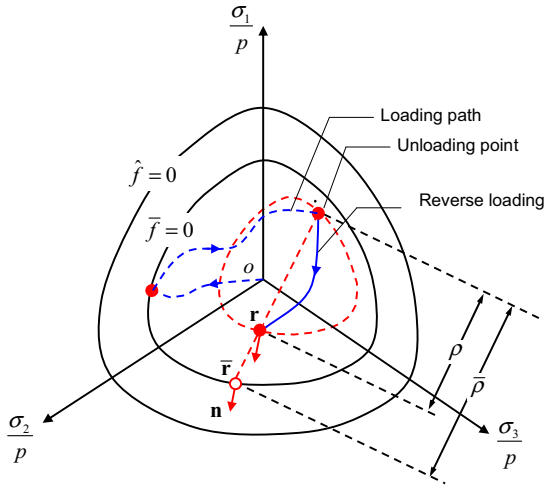

Fig. 1. The bounding surface model in deviatoric stress ratio space.

Author's personal copy

The numerical integration of this model is conducted in three steps:

Step 1. *Compute the state variables at the last time step.*
The pressure is computed using the last converged stress $\boldsymbol{\sigma}_n$ as:

$$p = \frac{1}{3} tr(\boldsymbol{\sigma}_n) = \frac{1}{3}(\boldsymbol{\sigma}_n : \mathbf{I}) \tag{6}$$

The deviatoric stress ratio is defined as

$$\mathbf{r} \equiv \frac{\boldsymbol{\sigma}_n}{p} - \mathbf{I} \tag{7}$$

The stress ratio invariant is defined as

$$R = \sqrt{\mathbf{r} : \mathbf{r}} \tag{8}$$

Based on the comparison of the stress ratio invariant R and the maximum ratio invariant R_m at maximum prestress memory bounding surface $\bar{f} = 0$, the mapping center $\boldsymbol{\alpha}$, the distance ρ and $\overline{\rho}$, and the unit vector $\mathbf{n}$ normal to $\bar{f} = 0$ are computed as follows:
If $R \geq R_m$, the current step is a virgin loading step, and

$$\boldsymbol{\alpha} = 0,\ R_m = R,\ \mathbf{n} = \mathbf{r}/R,\ \bar{\mathbf{r}} = \mathbf{r},\ \overline{\rho} = R_m,\ \rho = R \tag{9}$$

Otherwise, the current step is a reloading step, and

$$\rho = \sqrt{(\mathbf{r} - \boldsymbol{\alpha}) : (\mathbf{r} - \boldsymbol{\alpha})} \tag{10}$$

$$\overline{\rho} = \beta + \sqrt{\beta^2 + R_m^2 - \boldsymbol{\alpha} : \boldsymbol{\alpha}},\ \text{where } \beta = \frac{-(\mathbf{r} - \boldsymbol{\alpha}) : \boldsymbol{\alpha}}{\sqrt{(\mathbf{r} - \boldsymbol{\alpha}) : (\mathbf{r} - \boldsymbol{\alpha})}} \tag{11}$$

$$\mathbf{n} = \bar{\mathbf{r}} / \sqrt{\bar{\mathbf{r}} : \bar{\mathbf{r}}} = \bar{\mathbf{r}} / R_m,\ \text{where } \bar{\mathbf{r}} = \boldsymbol{\alpha} + \frac{\overline{\rho}}{\rho}(\mathbf{r} - \boldsymbol{\alpha}) \tag{12}$$

Step 2. *Compute the hypoelastic and hypoplastic moduli.*
The hypoelastic shear modulus G, the hypoelastic bulk modulus K, the plastic shear modulus H_r, and the plastic bulk modulus K_r are computed respectively as [23,19]:

$$G = p_a G_0 \frac{(2.973 - e_{in})^2}{1 + e_{in}} \sqrt{\frac{p}{p_a}} \tag{13}$$

$$K = \frac{2G(1+\nu)}{3(1-2\nu)} \tag{14}$$

$$H_r = G h_r \left(\frac{R_f}{R_m} \left(\frac{\rho}{\overline{\rho}} \right)^{-\tilde{m}} - 1 \right) \tag{15}$$

$$K_r = K / w \tag{16}$$

where p_a denotes the atmospheric pressure, G_0 is a nondimensional constant parameter, e_{in} is the initial void ratio, ν is Poisson's ratio, $\tilde{m} = 2R_m/\overline{\rho}$, and h_r is model parameter. The variable w is defined as an interpolation between the value w_m for monotonic loading and the value w_r for cyclic loading as follows:

$$w = w_r + (w_m - w_r) \left(\frac{\rho}{\overline{\rho}} \right)^{\tilde{n}} \tag{17}$$

where $\tilde{n}$ is a constant that is usually taken in the range $\tilde{n} = 20 \sim 30$, and

$$w_m = \frac{1}{k_r} \left(\frac{p}{p_m} \right)^a \left(\frac{R_m}{R_f} \right)^b \left(\frac{R_p - R_m}{R_f - R_m} \right) \tag{18}$$

$$w_r = \left(\frac{R_m}{R_f} \right)^{d + 2\sin(\pi p / p_m)} (1 - e^{1 - p/p_{\min}}) \tag{19}$$

where parameters a, b, d, and k_r are model constants. R_p is the stress ratio invariant delimitating the phase transformation between volumetric contraction and dilation. It is defined as

$$R_p = R_f \exp\left(sign(\psi)\, m\, |\psi|^n \right) \tag{20}$$

where m and n are constants used to calibrate the phase transformation line. The phase transformation line is assumed to be dependent on a state parameter ψ, which is defined as the difference between e_{in} and the critical void ratio e_c as follows:

$$\psi = e_{in} - e_c \tag{21}$$

The critical void ratio e_c is uniquely determined by the effective confining pressure. The critical-state line can be defined by constants γ, λ and ξ in the e–p space as follows:

$$e_c = \gamma - \lambda \left(\frac{p}{p_a} \right)^{\xi} \tag{22}$$

It is worth mentioning that the state-dependent dilatancy formulation in Eq. (20) effectively bounds the dilatancy behavior at the critical state limit. A detailed discussion of this can be found in the literature [20,21].
Step 3. *Compute the current stress based on loading or unloading conditions.*
Given a strain increment $\Delta\boldsymbol{\varepsilon}$, a trial elastic stress increment $\Delta\boldsymbol{\sigma}^{tr}$ is computed as:

$$\Delta\sigma^{tr} = \mathbf{C}^e : \Delta\boldsymbol{\varepsilon} \tag{23}$$

where $\mathbf{C}^e$ denotes the tensor of elastic moduli, which in the case of isotropic elasticity can be expressed as $C^e_{ijkl} = (K - \frac{2}{3}G)\delta_{ij}\delta_{kl} + G(\delta_{ik}\delta_{jl} + \delta_{il}\delta_{jk})$. Correspondingly, the pressure increment is

$$\Delta p = \frac{1}{3} \Delta\boldsymbol{\sigma}^{tr} : \mathbf{I} \tag{24}$$

The loading index is computed as:

$$L = p\Delta\mathbf{r} : \mathbf{n} = \left(\Delta\boldsymbol{\sigma}^{tr} - \frac{\Delta p}{p} \boldsymbol{\sigma}_n \right) : \mathbf{n} \tag{25}$$

If $L \geq 0$, this step is a loading step, and so the current stress can be computed as

$$\boldsymbol{\sigma}_{n+1} = \boldsymbol{\sigma}_n + \Delta\boldsymbol{\sigma}^{tr} - \frac{2G}{C_2} \mathbf{p}^r \otimes \mathbf{Q}^p : \Delta\boldsymbol{\varepsilon} = \boldsymbol{\sigma}_n + \mathbf{C}^{ep} : \Delta\boldsymbol{\varepsilon} \tag{26}$$

where $\otimes$ is the tensor product operator defined as $\boldsymbol{A} \otimes \boldsymbol{B} = A_{ij}B_{kl}$, and

$$\mathbf{p}^r = \mathbf{n} + \frac{1}{2} \frac{K}{K_r} \frac{H_r}{G} \mathbf{I} \tag{27}$$

$$Q^p = B_p \boldsymbol{n} - B_r \boldsymbol{I} \tag{28}$$

$$C_2 = A_r B_p - A_p B_r, A_r = \frac{1}{2} \frac{H_r}{G} + 1, A_p = \frac{H_r}{K_r}, B_r = \mathbf{r} : \mathbf{n}, B_p = 2\frac{G}{K} \tag{29}$$

The elasto-plastic tangent modulus is computed as:

$$\mathbf{C}^{ep} = \mathbf{C} - \frac{2G}{C_2} \mathbf{p}^r \otimes \mathbf{Q}^p \tag{30}$$

Author's personal copy

On the other hand, if $L<0$, this step is an elastic unloading step. In this case, the current stress is computed as

$$\boldsymbol{\sigma}_{n+1}=\boldsymbol{\sigma}_n+\Delta\boldsymbol{\sigma}^{tr}=\boldsymbol{\sigma}_n+\mathbf{C}^e:\Delta\boldsymbol{\varepsilon} \tag{31}$$

After the instantaneous unloading step, the mapping center $\boldsymbol{\alpha}$ is updated to $\boldsymbol{\sigma}_n$. Step 3 is repeated for subsequent stress computation.

3. The response sensitivity algorithm based on the direct differentiation method

Response sensitivity is defined as the first derivative of a response quantity r (e.g., displacement, strain, stress) with respect to a sensitivity parameter θ, i.e., $dr/d\theta$. The sensitivity parameter could be a geometric, material or loading parameter. In general, the scalar response quantity $r(\theta)=r(\boldsymbol{f}(\theta),\theta)$ depends on the parameter θ both explicitly and implicitly through the vector function $\boldsymbol{f}(\theta)$. The DDM-based response sensitivities are computed after convergence of each time or loading step in nonlinear FE response analysis. This requires consistent differentiation of the FE algorithm for the response-only computation with respect to each sensitivity parameter θ. Consequently, the response sensitivity computation algorithm involves various hierarchical levels of FE response analysis: (1) the structure/system level, (2) the element level or section level, and (3) the material level. Details about the DDM-based sensitivity formulations in classical displacement-based, force-based and mixed finite element methods can be found in the literature [7–10,24].

3.1. Displacement-based FE response sensitivity analysis using DDM

After spatial discretization using the finite element method, the equations of motion of a structural system can be represented by the following nonlinear differential equation:

$$\mathbf{M}(\theta)\ddot{\mathbf{u}}(t,\theta)+\mathbf{C}(\theta)\dot{\mathbf{u}}(t,\theta)+\mathbf{R}(\mathbf{u}(t,\theta),\theta)=\mathbf{F}(t,\theta) \tag{32}$$

where t is time, θ is a scalar sensitivity parameter, $\mathbf{u}(t)$ is a vector of nodal displacements, $\mathbf{M}$ is the mass matrix, $\mathbf{C}$ is the damping matrix, $\mathbf{R}(\mathbf{u},t)$ is a history-dependent internal resisting force vector, $\mathbf{F}(t)$ is the applied dynamic load vector, and $\dot{\mathbf{u}}$ and $\ddot{\mathbf{u}}$ denote, respectively, the first and second derivatives of $\mathbf{u}$ with respect to time. Without loss of generality, Eq. (32) can be integrated numerically using time-stepping methods such as the well-known Newmark-β method [25]. The system of equations can be solved using the Newton–Raphson iteration procedure, which consists of solving a linearized system of equations at each iteration. In the following discretized format, a subscript n+1 is used to denote the variables at the time step n+1. Assuming that $\mathbf{u}_{n+1}$ is the converged solution for the current time step t_{n+1}, and recognizing that $\mathbf{R}(\mathbf{u}_{n+1})=\mathbf{R}(\mathbf{u}_{n+1}(\theta),\theta)$ depends on θ explicitly and implicitly through $\mathbf{u}_{n+1}$, we obtain the following response sensitivity equation at the structural level using the chain rule of differentiation [2,5]:

$$\left[\frac{1}{\beta(\Delta t)^2}\mathbf{M}+\frac{\alpha}{\beta(\Delta t)}\mathbf{C}+(\mathbf{K_T})^{\text{stat}}_{n+1}\right]\frac{d\mathbf{u}_{n+1}}{d\theta}=\frac{d\tilde{\mathbf{F}}_{n+1}}{d\theta}-\frac{\partial\mathbf{R}(\mathbf{u}_{n+1}(\theta),\theta)}{\partial\theta}\bigg|_{\mathbf{u}_{n+1}}-\left(\frac{1}{\beta(\Delta t)^2}\frac{d\mathbf{M}}{d\theta}+\frac{\alpha}{\beta(\Delta t)}\frac{d\mathbf{C}}{d\theta}\right)\mathbf{u}_{n+1} \tag{33}$$

where

$$\frac{d\tilde{\mathbf{F}}_{n+1}}{d\theta}=\frac{d\mathbf{F}_{n+1}}{d\theta}+\frac{d\mathbf{M}}{d\theta}\left[\frac{1}{\beta(\Delta t)^2}\mathbf{u}_n+\frac{1}{\beta(\Delta t)}\dot{\mathbf{u}}_n-\left(1-\frac{1}{2\beta}\right)\ddot{\mathbf{u}}_n\right]+\mathbf{M}\left[\frac{1}{\beta(\Delta t)^2}\frac{d\mathbf{u}_n}{d\theta}+\frac{1}{\beta(\Delta t)}\frac{d\dot{\mathbf{u}}_n}{d\theta}-\left(1-\frac{1}{2\beta}\right)\frac{d\ddot{\mathbf{u}}_n}{d\theta}\right]$$
$$+\frac{d\mathbf{C}}{d\theta}\left[\frac{\alpha}{\beta(\Delta t)}\mathbf{u}_n-\left(1-\frac{\alpha}{\beta}\right)\dot{\mathbf{u}}_n-(\Delta t)\left(1-\frac{\alpha}{2\beta}\right)\ddot{\mathbf{u}}_n\right]+\mathbf{C}\left[\frac{\alpha}{\beta(\Delta t)}\frac{d\mathbf{u}_n}{d\theta}-\left(1-\frac{\alpha}{\beta}\right)\frac{d\dot{\mathbf{u}}_n}{d\theta}-(\Delta t)\left(1-\frac{\alpha}{2\beta}\right)\frac{d\ddot{\mathbf{u}}_n}{d\theta}\right] \tag{34}$$

In Eq. (33), α and β are Newmark integration parameters, and $(\mathbf{K_T})^{\text{stat}}_{n+1}$ denotes the static algorithmic (consistent) tangent stiffness matrix of the structure/system, which is defined as the assembly of the consistent tangent stiffness matrices of the elements as

$$(\mathbf{K_T})^{\text{stat}}_{n+1}=\frac{\partial\mathbf{R}(\mathbf{u}_{n+1})}{\partial\mathbf{u}_{n+1}}=\mathop{\mathbf{A}}_{e=1}^{nel}\left(\int_{\Omega^e}\mathbf{B}^T\mathbf{C}^{alg}_{n+1}\mathbf{B}\;d\Omega^e\right) \tag{35}$$

where $\mathbf{A}_{n=1}^{nel}()$ denotes the direct stiffness assembly operator, *nel* represents the number of elements in the FE model, $\mathbf{B}$ is the strain–displacement transformation matrix, $\mathbf{C}^{alg}_{n+1}$ denotes the algorithmic (consistent) tangent moduli obtained through consistent linearization of the constitutive law integration scheme [26,27], i.e.,

$$\mathbf{C}^{alg}_{n+1}=\frac{\partial\boldsymbol{\sigma}_{n+1}(\boldsymbol{\sigma}_n,\boldsymbol{\varepsilon}_n,\boldsymbol{\varepsilon}_{n+1}\ldots)}{\partial\boldsymbol{\varepsilon}_{n+1}} \tag{36}$$

where $\boldsymbol{\sigma}_{n+1}$ is the stress at current time step t_{n+1}. Since an explicit integration method is used in this model, i.e., $\boldsymbol{\sigma}_{n+1}=\boldsymbol{\sigma}_n+\mathbf{C}^{ep}:\Delta\boldsymbol{\varepsilon}$, it is straightforward to show that the consistent tangent modulus for the presented bounding surface plasticity material model is the same as the continuum tangent moduli as shown in Eq. (30), i.e., $\mathbf{C}^{alg}_{n+1}=\mathbf{C}^{ep}$. In addition, the DDM sensitivity results are verified by using FDM results, showing that the consistent tangent modulus is correct.

The second term on the right-hand side of Eq. (33) represents the partial derivative of the internal resisting force vector, $\mathbf{R}(\mathbf{u}_{n+1})$, with respect to the sensitivity parameter θ under the condition that the nodal displacement vector $\mathbf{u}_{n+1}$ remains fixed. It is computed through the direct stiffness assembly of the element resisting force derivatives as:

$$\frac{\partial\mathbf{R}(\mathbf{u}_{n+1})}{\partial\theta}\bigg|_{\mathbf{u}_{n+1}}=\mathop{\mathbf{A}}_{e=1}^{nel}\left(\int_{\Omega^e}\mathbf{B}^T(\mathbf{x})\frac{\partial\boldsymbol{\sigma}(\boldsymbol{\varepsilon}_{n+1}(\theta),\theta)}{\partial\theta}\bigg|_{\boldsymbol{\varepsilon}_{n+1}}d\Omega^e\right) \tag{37}$$

Although the conditional stress sensitivity $\frac{\partial\boldsymbol{\sigma}(\boldsymbol{\varepsilon}_{n+1}(\theta),\theta)}{\partial\theta}\Big|_{\boldsymbol{\varepsilon}_{n+1}}$ is required to solve Eq. (33) for the unknown $\frac{d\mathbf{u}_{n+1}}{d\theta}$, only the formulation of unconditional stress sensitivities $\frac{\partial\boldsymbol{\sigma}(\boldsymbol{\varepsilon}_{n+1}(\theta),\theta)}{\partial\theta}$ is presented in the following section. The conditional stress sensitivity is obtained as a special case of the unconditional one by setting the term $\frac{\partial\boldsymbol{\varepsilon}_{n+1}}{\partial\theta}=0$ in the derivation.

3.2. A stress sensitivity computation algorithm for the bounding surface plasticity model

Without loss of generality, fourteen material parameters are considered as potential sensitivity parameters in this paper: the reference shear modulus G_0 and the initial void ratio e_{in} in Eq. (13), Poisson's ratio ν in Eq. (14), the constants γ,λ, and ξ in Eq. (22), the failure deviatoric stress ratio R_f, the constants m and n in Eq. (20), the constants a, b, d, and k_r in Eqs. (18) and (19), and the constant h_r in Eq. (15). Following the stress computation process in steps 1–3 in Section 2.2, the sensitivities of each intermediate variable are derived as follows.

Step 1. *Compute the sensitivities of the state variables at the last converged time step.*

Author's personal copy

Differentiating Eqs. (6)–(12) with respect to parameter θ gives

$$\frac{\partial p}{\partial \theta}=\frac{1}{3}\left(\frac{\partial \boldsymbol{\sigma}_n}{\partial \theta}:\mathbf{I}\right) \tag{38}$$

$$\frac{\partial \mathbf{r}}{\partial \theta}=\frac{1}{p}\frac{\partial \boldsymbol{\sigma}_n}{\partial \theta}-\frac{\boldsymbol{\sigma}_n}{p^2}\frac{\partial p}{\partial \theta} \tag{39}$$

$$\frac{\partial R}{\partial \theta}=\frac{1}{R}\mathbf{r}:\frac{\partial \mathbf{r}}{\partial \theta} \tag{40}$$

If $R \geq R_m$

$$\frac{\partial \boldsymbol{\alpha}}{\partial \theta}=0,\frac{\partial R_m}{\partial \theta}=\frac{\partial R}{\partial \theta},\frac{\partial \mathbf{n}}{\partial \theta}=\frac{1}{R}\frac{\partial \mathbf{r}}{\partial \theta}-\frac{\mathbf{r}}{R^2}\frac{\partial R}{\partial \theta},\frac{\partial \overline{\mathbf{r}}}{\partial \theta}=\frac{\partial \mathbf{r}}{\partial \theta},\frac{\partial \overline{\rho}}{\partial \theta}=\frac{\partial R_m}{\partial \theta},\frac{\partial \rho}{\partial \theta}=\frac{\partial R}{\partial \theta} \tag{41}$$

otherwise

$$\frac{\partial \rho}{\partial \theta}=\frac{1}{\rho}\left(\frac{\partial \mathbf{r}}{\partial \theta}-\frac{\partial \boldsymbol{\alpha}}{\partial \theta}\right):(\mathbf{r}-\boldsymbol{\alpha}) \tag{42}$$

$$\frac{\partial \beta}{\partial \theta}=\frac{1}{\rho}\left[\left(\frac{\partial \boldsymbol{\alpha}}{\partial \theta}-\frac{\partial \mathbf{r}}{\partial \theta}\right):\boldsymbol{\alpha}+(\boldsymbol{\alpha}-\mathbf{r}):\frac{\partial \boldsymbol{\alpha}}{\partial \theta}\right]-\frac{\partial \rho}{\partial \theta}\frac{\beta}{\rho} \tag{43}$$

$$\frac{\partial \overline{\rho}}{\partial \theta}=\frac{\partial \beta}{\partial \theta}+\frac{1}{\sqrt{\beta^2+R_m^2-\boldsymbol{\alpha}:\boldsymbol{\alpha}}}\left(\beta\cdot\frac{\partial \beta}{\partial \theta}+R_m\cdot\frac{\partial R_m}{\partial \theta}-\boldsymbol{\alpha}:\frac{\partial \boldsymbol{\alpha}}{\partial \theta}\right) \tag{44}$$

$$\frac{\partial \overline{\mathbf{r}}}{\partial \theta}=\frac{\partial \boldsymbol{\alpha}}{\partial \theta}+\frac{\overline{\rho}}{\rho}\left(\frac{\partial \mathbf{r}}{\partial \theta}-\frac{\partial \boldsymbol{\alpha}}{\partial \theta}\right)+\frac{1}{\rho^2}\left(\frac{\partial \overline{\rho}}{\partial \theta}\rho-\overline{\rho}\frac{\partial \rho}{\partial \theta}\right)(\mathbf{r}-\boldsymbol{\alpha}) \tag{45}$$

$$\frac{\partial \mathbf{n}}{\partial \theta}=\frac{1}{R_m}\frac{\partial \overline{\mathbf{r}}}{\partial \theta}-\frac{\mathbf{n}}{(R_m)^2}\left(\overline{\mathbf{r}}:\frac{\partial \overline{\mathbf{r}}}{\partial \theta}\right) \tag{46}$$

Step 2. Compute the sensitivities of the moduli needed for current step.

Differentiating Eqs. (13) to (22) with respect to parameter θ gives

$$\frac{\partial G}{\partial \theta}=\frac{G}{G_0}\frac{\partial G_0}{\partial \theta}-\left(\frac{G}{(1+e_{in})}+\frac{2G}{(2.973-e_{in})}\right)\frac{\partial e_{in}}{\partial \theta}+\frac{G}{2p}\frac{\partial p}{\partial \theta} \tag{47}$$

$$\frac{\partial K}{\partial \theta}=\frac{K}{G}\frac{\partial G}{\partial \theta}+\left(\frac{K}{(1+\nu)}+\frac{2K}{(1-2\nu)}\right)\frac{\partial \nu}{\partial \theta} \tag{48}$$

$$\frac{\partial e_c}{\partial \theta}=\frac{\partial \gamma}{\partial \theta}-\frac{\partial \lambda}{\partial \theta}\left(\frac{p}{p_a}\right)^{\xi}-\lambda\left[\frac{\xi}{p_a}\left(\frac{p}{p_a}\right)^{\xi-1}\frac{\partial p}{\partial \theta}+\left(\frac{p}{p_a}\right)^{\xi}\ln\left(\frac{p}{p_a}\right)\frac{\partial \xi}{\partial \theta}\right] \tag{49}$$

$$\frac{\partial \psi}{\partial \theta}=\frac{\partial e_{in}}{\partial \theta}-\frac{\partial e_c}{\partial \theta} \tag{50}$$

$$\frac{\partial R_p}{\partial \theta}=\frac{R_p}{R_f}\frac{\partial R_f}{\partial \theta}+R_p\cdot sign(\psi)\left[\frac{\partial m}{\partial \theta}\ |\psi|^n+m\left(n\ |\psi|^{n-1}\ sign(\psi)\ \frac{\partial \psi}{\partial \theta}+\ln|\psi\ \|\psi|^n\ \frac{\partial n}{\partial \theta}\right)\right] \tag{51}$$

$$\begin{aligned}\frac{\partial w_m}{\partial \theta}=&w_m\left[\ln\left(\frac{p}{p_m}\right)\frac{\partial a}{\partial \theta}+\frac{a}{p_m}\frac{}{p}\left(\frac{\partial p}{\partial \theta}p_m-\frac{\partial p_m}{\partial \theta}p\right)\right]\\&+w_m\left[\ln\left(\frac{R_m}{R_{\max}}\right)\frac{\partial b}{\partial \theta}+\frac{b}{R_m}\frac{\partial R_m}{\partial \theta}-\frac{b}{R_{\max}}\frac{\partial R_{\max}}{\partial \theta}\right]\\&+\frac{w_m}{(R_p-R_m)}\left(\frac{\partial R_p}{\partial \theta}-\frac{\partial R_m}{\partial \theta}\right)\\&-\frac{w_m}{(R_{\max}-R_m)}\left(\frac{\partial R_{\max}}{\partial \theta}-\frac{\partial R_m}{\partial \theta}\right)-w_m\frac{1}{k_r}\frac{\partial k_r}{\partial \theta}\end{aligned} \tag{52}$$

$$\begin{aligned}\frac{\partial w_r}{\partial \theta}=&\left(\frac{R_m}{R_{\max}}\right)^{\left[d+2\sin\left(\frac{\pi p}{p_m}\right)\right]}\left(\frac{1}{p_{\min}}e^{1-\frac{p}{p_{\min}}}\frac{\partial p}{\partial \theta}\right)\\&+w_r\ln\left(\frac{R_m}{R_{\max}}\right)\left[\frac{\partial d}{\partial \theta}+2\cos\left(\frac{\pi p}{p_m}\right)\frac{\pi}{(p_m)^2}\left(\frac{\partial p}{\partial \theta}p_m-\frac{\partial p_m}{\partial \theta}p\right)\right]\\&+\frac{w_r}{(R_{\max})^2}\left[d+2\sin\left(\frac{\pi p}{p_m}\right)\right]\left(\frac{R_{\max}}{R_m}\right)\left(\frac{\partial R_m}{\partial \theta}R_{\max}-\frac{\partial R_{\max}}{\partial \theta}R_m\right)\end{aligned} \tag{53}$$

$$\begin{aligned}\frac{\partial w}{\partial \theta}=&\frac{\partial w_r}{\partial \theta}+\left(\frac{\partial w_m}{\partial \theta}-\frac{\partial w_r}{\partial \theta}\right)\left(\frac{\rho}{\overline{\rho}}\right)^{\tilde{n}}\\&+(w_m-w_r)\cdot\frac{\tilde{n}}{(\overline{\rho})^2}\left(\frac{\rho}{\overline{\rho}}\right)^{\tilde{n}-1}\left(\frac{\partial \rho}{\partial \theta}\overline{\rho}-\frac{\partial \overline{\rho}}{\partial \theta}\rho\right)\end{aligned} \tag{54}$$

$$\frac{\partial K_r}{\partial \theta}=\frac{1}{w^2}\left(\frac{\partial K}{\partial \theta}w-K\frac{\partial w}{\partial \theta}\right) \tag{55}$$

$$\begin{aligned}\frac{\partial H_r}{\partial \theta}=&H_r\left(\frac{1}{G}\frac{\partial G}{\partial \theta}+\frac{1}{h_r}\frac{\partial h_r}{\partial \theta}\right)+Gh_r\left(\frac{\left(\frac{\partial R_f}{\partial \theta}R_m-R_f\frac{\partial R_m}{\partial \theta}\right)}{(R_m)^2}\left(\frac{\rho}{\overline{\rho}}\right)^{-\tilde{m}}\right.\\&\left.-\frac{R_f}{R_m}\left[\left(\frac{\rho}{\overline{\rho}}\right)^{-\tilde{m}}\cdot\ln\left(\frac{\rho}{\overline{\rho}}\right)\frac{\partial \tilde{m}}{\partial \theta}+\frac{\tilde{m}}{(\overline{\rho})^2}\left(\frac{\rho}{\overline{\rho}}\right)^{-\tilde{m}-1}\left(\frac{\partial \rho}{\partial \theta}\overline{\rho}-\frac{\partial \overline{\rho}}{\partial \theta}\rho\right)\right]\right)\end{aligned} \tag{56}$$

Step 3. Compute the sensitivities of the current stress.

Differentiating Eqs. (23) and (24) with respect to the sensitivity parameter θ gives,

$$\frac{\partial \Delta\boldsymbol{\sigma}^{tr}}{\partial \theta}=\frac{\partial \mathbf{C}}{\partial \theta}:\Delta\boldsymbol{\varepsilon}+\mathbf{C}:\frac{\partial \Delta\boldsymbol{\varepsilon}}{\partial \theta} \tag{57}$$

$$\frac{\partial \Delta p}{\partial \theta}=\frac{1}{3}\left(\frac{\partial \Delta\boldsymbol{\sigma}^{tr}}{\partial \theta}:\mathbf{I}\right) \tag{58}$$

If $L \geq 0$ (a loading step), differentiating Eqs. (7), (12), (26)–(29) with respect to θ yields

$$\frac{\partial A_r}{\partial \theta}=\frac{1}{2G}\frac{\partial H_r}{\partial \theta}-\frac{1}{2}\frac{H_r}{G^2}\frac{\partial G}{\partial \theta} \tag{59}$$

$$\frac{\partial A_p}{\partial \theta}=\frac{1}{K_r}\frac{\partial H_r}{\partial \theta}+H_r\frac{\partial (1/K_r)}{\partial \theta} \tag{60}$$

$$\frac{\partial \mathbf{n}}{\partial \theta}=\frac{1}{\sqrt{\overline{\mathbf{r}}:\overline{\mathbf{r}}}}\frac{\partial \overline{\mathbf{r}}}{\partial \theta}-\left(\overline{\mathbf{r}}:\frac{\partial \overline{\mathbf{r}}}{\partial \theta}\right)\frac{\mathbf{n}}{\overline{\mathbf{r}}:\overline{\mathbf{r}}} \tag{61}$$

$$\frac{\partial \mathbf{r}}{\partial \theta}=\frac{1}{p}\frac{\partial \boldsymbol{\sigma}_n}{\partial \theta}-\frac{\boldsymbol{\sigma}_n}{p^2}\frac{\partial p}{\partial \theta} \tag{62}$$

$$\frac{\partial B_r}{\partial \theta}=\frac{\partial \mathbf{r}}{\partial \theta}:\mathbf{n}+\mathbf{r}:\frac{\partial \mathbf{n}}{\partial \theta} \tag{63}$$

$$\frac{\partial B_p}{\partial \theta}=\frac{2}{K}\frac{\partial G}{\partial \theta}-\frac{2G}{K^2}\frac{\partial K}{\partial \theta} \tag{64}$$

$$\frac{\partial C_2}{\partial \theta}=\frac{\partial A_r}{\partial \theta}B_p+A_r\frac{\partial B_p}{\partial \theta}-\frac{\partial A_p}{\partial \theta}B_r-A_p\frac{\partial B_r}{\partial \theta} \tag{65}$$

$$\frac{\partial \mathbf{Q}^p}{\partial \theta}=\frac{\partial B_p}{\partial \theta}\mathbf{n}+B_p\frac{\partial \mathbf{n}}{\partial \theta}-\frac{\partial B_r}{\partial \theta}\mathbf{I} \tag{66}$$

$$\frac{\partial \mathbf{p}^r}{\partial \theta}=\frac{\partial \mathbf{n}}{\partial \theta}+\frac{1}{2}\left(\frac{1}{K_r}\frac{H_r}{G}\frac{\partial K}{\partial \theta}+\frac{K}{K_r}\frac{1}{G}\frac{\partial H_r}{\partial \theta}-\frac{K}{(K_r)^2}\frac{H_r}{G}\frac{\partial K_r}{\partial \theta}-\frac{K}{K_r}\frac{H_r}{G^2}\frac{\partial G}{\partial \theta}\right)\mathbf{I} \tag{67}$$

$$\begin{aligned}\frac{\partial \boldsymbol{\sigma}_{n+1}}{\partial \theta}=&\frac{\partial \boldsymbol{\sigma}_n}{\partial \theta}+\frac{\partial \Delta\boldsymbol{\sigma}^{tr}}{\partial \theta}-2\ \frac{\partial G}{\partial \theta}\frac{1}{C_2}\mathbf{p}^r\otimes\mathbf{Q}^p:\Delta\boldsymbol{\varepsilon}-\frac{2G}{C_2}\ \frac{\partial \mathbf{p}^r}{\partial \theta}\otimes\mathbf{Q}^p:\Delta\boldsymbol{\varepsilon}\\&-\frac{2G}{C_2}\left(\frac{\partial \mathbf{Q}^p}{\partial \theta}:\Delta\boldsymbol{\varepsilon}+\mathbf{Q}^p:\frac{\partial \Delta\boldsymbol{\varepsilon}}{\partial \theta}-\frac{1}{C_2}\frac{\partial C_2}{\partial \theta}\mathbf{Q}^p:\Delta\boldsymbol{\varepsilon}\right)\mathbf{p}^r\end{aligned} \tag{68}$$

Author's personal copy

On the other hand, if $L<0$ (an elastic unloading step), the differentiation of Eq. (31) with respect to θ reads

$$\frac{\partial \boldsymbol{\sigma}_{n+1}}{\partial \theta} = \frac{\partial \boldsymbol{\sigma}_n}{\partial \theta} + \frac{\partial \Delta \boldsymbol{\sigma}_n^{tr}}{\partial \theta} \tag{69}$$

From Eqs. (38)–(69), the unconditional stress sensitivity $\frac{\partial \boldsymbol{\sigma}_{n+1}(\boldsymbol{\varepsilon}_{n+1}(\theta),\theta)}{\partial \theta}$ can be obtained. The conditional stress sensitivity $\left.\frac{\partial \boldsymbol{\sigma}_{n+1}(\boldsymbol{\varepsilon}_{n+1}(\theta),\theta)}{\partial \theta}\right|_{\boldsymbol{\varepsilon}_{n+1}}$ can be also computed following Eqs. (38)–(69) by simply setting $\frac{\partial \boldsymbol{\varepsilon}_{n+1}}{\partial \theta}$ to zero in Eq. (57), i.e., $\frac{\partial \Delta \boldsymbol{\varepsilon}}{\partial \theta} = \frac{\partial \boldsymbol{\varepsilon}_{n+1}}{\partial \theta} - \frac{\partial \boldsymbol{\varepsilon}_n}{\partial \theta} = -\frac{\partial \boldsymbol{\varepsilon}_n}{\partial \theta}$, since $\boldsymbol{\varepsilon}_{n+1}$ is assumed to be fixed in the conditional case. Then from Eq. (37), $\left.\frac{\partial \mathbf{R}(\mathbf{u}_{n+1})}{\partial \theta}\right|_{\mathbf{u}_{n+1}}$ can be computed and finally the unknown $\frac{d\mathbf{u}_{n+1}}{d\theta}$ can be solved by Eq. (33).

4. Numerical examples

In this section, two examples are presented to verify the above DDM algorithm and illustrate its application in modeling liquefiable soils. In these examples, the soils are considered fully saturated and undrained based on the following assumptions: (a) The process of water seepage is much slower than that of the earthquake loading, thus can be ignored; (b) Volumetric modulus of water is much larger than that of soil, thus water is considered as incompressible. The soil-water interaction can be modeled by prescribing the following "equalDOF" constraints: after the initial pressure is applied, the volume of each element is kept constant by fixing the vertical displacement of all nodes and imposing the same horizontal displacements to each pair of nodes at the same depth. Therefore, the volume soil element and the volume of water inside soil keep constant during earthquake shaking. For a horizontally layered soil subject to horizontal earthquake loading, the total pressure at any point keeps constant and is equal to the initial pressure. The soil effective pressure is computed by using the bounding surface soil model presented herein. Thus, the pore water pressure can be obtained as the difference between the initial total pressure and the soil effective pressure, and it is not modeled as an independent variable. Compared to using a fully coupled fluid–soil element, i.e., u–p formulation [28], the limitation of this method is that it cannot realistically simulate the post-liquefaction process, which involves the water drainage and pore water pressure dissipation.

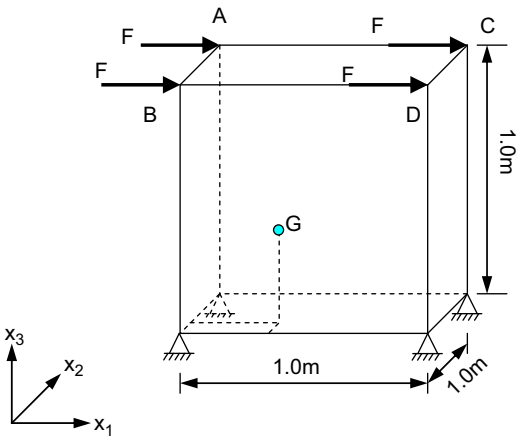

Fig. 2. Solid block of sand subjected to horizontal quasi-static cyclic loading (loads applied for initial pressure are omitted for clarity).

4.1. A sand block subjected to quasi-static cyclic loading

In this example, a soil block with dimensions 1 m × 1 m × 1 m (see Fig. 2) subjected to quasi-static cyclic loading is studied to validate the bounding surface model and its sensitivity algorithm. The block is modeled using one eight-node, trilinear isoparametric brick element with eight integration points. The following parameters are used in the bounding surface model for a sand with initial void ratio $e_{in}=0.818$, reference shear modulus $G_0=200$ Pa, and Poisson's ratio $\nu=0.05$. Other model constants used are $\gamma=0.934$,$\lambda=0.019$, and $\xi=0.7$ in Eq. (22); $R_f=1.0154$, $m=3.5$, and $n=0.75$ in Eq. (20); $k_r=0.5423$, $a=0.0$, $b=1.0$, and $d=1.9$ in Eqs. (18) and (19); and $h_r=0.1811$ in Eq. (15). The initial horizontal and vertical pressures are 1.2×10^5 Pa and 2.4×10^5 Pa, respectively. The above-mentioned "equalDOF" constraints are specified to model a plane-strain, undrained, simple-shear condition. The volume of the element remains constant during the loading. Each of the top nodes {A, B, C, D} is subjected to a cyclic load with magnitude $F=10^4$ N as shown in Fig. 2.

Fig. 3 shows the displacement response of node A (see Fig. 2) in the x_1-direction under the cyclic load. The shear stress vs. shear strain response at Gauss point G (see Fig. 2) is plotted in Fig. 4(a), where the starting point is marked by a circle. Fig. 4(b) plots the shear stress vs. the effective confining pressure p under cyclic loading. During the first few cycles, the soil exhibits shear-induced volumetric contraction such that p keeps reducing until the phase transformation line is reached. Then the soil exhibits dilative behavior and p increases accordingly. The repeated loading and unloading result in the distinctive "butterfly" loops in Fig. 4(b).

The DDM-based sensitivities of the displacement response $u(t)$ of node A in the x_1-direction to the model constant G_0, the initial void ratio e_{in}, and the failure deviatoric stress ratio R_f, are compared with the FFD-based sensitivities using different normalized perturbation $\Delta\theta/\theta=10^{-3}$, 10^{-4}, and 10^{-5}. The comparison results and the enlarged views of sections of interest are shown in Figs. 5–7. From these figures, it is clear that the FFD results converge asymptotically to the DDM results as $\Delta\theta/\theta$ changes from 10^{-3} to 10^{-5}. One can also see spikes in the sensitivity results in Figs. 6 and 7. A close inspection reveals that the spikes correspond to the phase transfer points, at which soils transform suddenly from volumetric contraction to dilation, and the plastic modulus K_r changes sign from positive to negative. Thus the first derivative of the response has a spike at the phase transfer point.

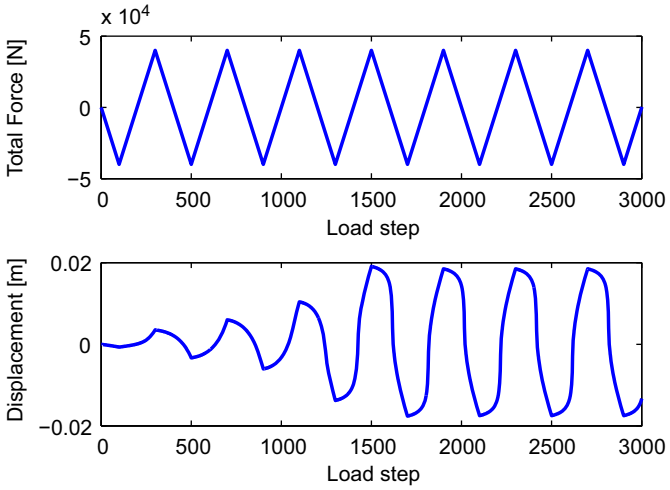

Fig. 3. Load history and displacement history at node A.

Author's personal copy

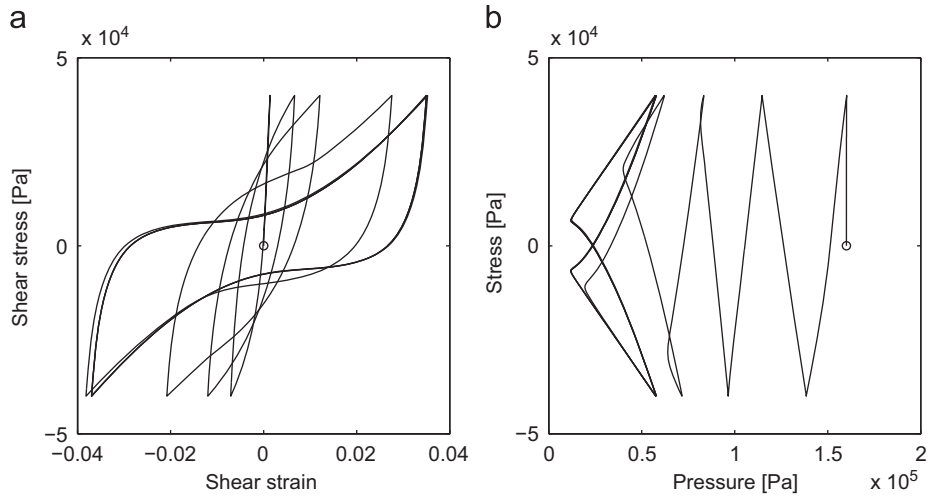

Fig. 4. Local responses at Gaussian point G under undrained cyclic loading. (a) Shear stress vs. strain responses and (b) shear stress vs. mean effective pressure.

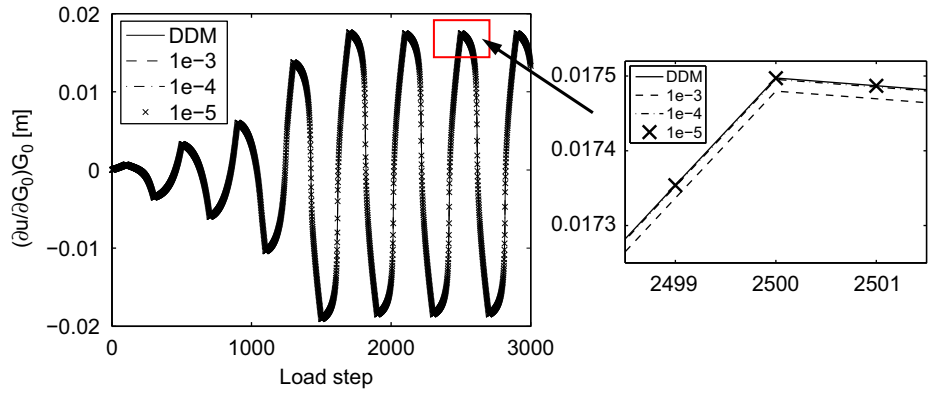

Fig. 5. Sensitivity of displacement of node A to G_0 using DDM vs. FFD with different perturbation levels

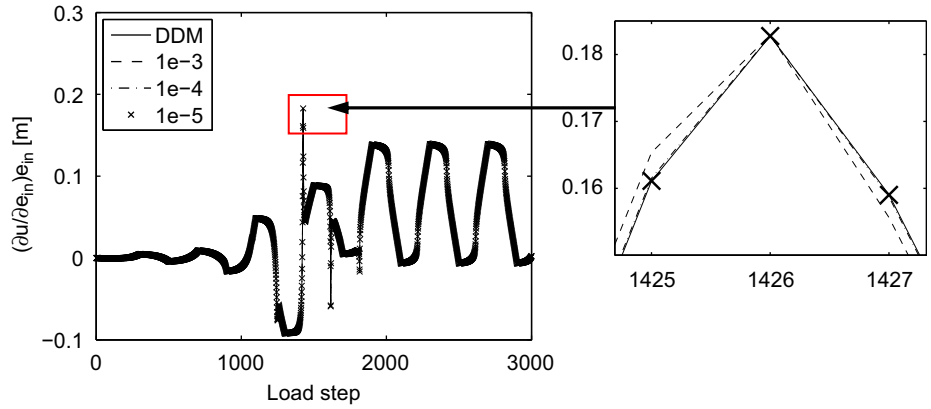

Fig. 6. Sensitivity of displacement of node A to e_{in} using DDM vs. FFD with different perturbation levels

4.2. *A multi-layered soil column subjected to earthquake excitation*

The second example investigates the response sensitivities of a multi-layered soil site located at Port Island in Kobe, Japan, subjected to earthquake loading. The soil there is composed of an 18 m thick layer of reclaimed sand on top of silty clay, sand and silt layers. The soil profile is illustrated in Fig. 8(a). The top layer of reclaimed sand underwent extensive liquefaction, lateral spreading, and liquefaction-induced settlement during an earthquake on January 17, 1995. Ground motion acceleration time histories have been recorded using a downhole array with stations at the ground surface, at 16 m, 32 m, and 82 m below ground surface, providing valuable information for studying the liquefaction phenomenon [29,30].

In this study, the soil column is discretized using two-dimensional plane-strain quadrilateral elements with a dimension of 1 to 2 m in vertical direction. The "equalDOF" constraints are prescribed so the soil column deforms under undrained simple-shear condition. The sand and clay materials are both modeled using the bounding surface model presented in this paper, and the material parameters are listed in Table 1. Gravity is first applied statically, which generates the initial confining pressure

Author's personal copy

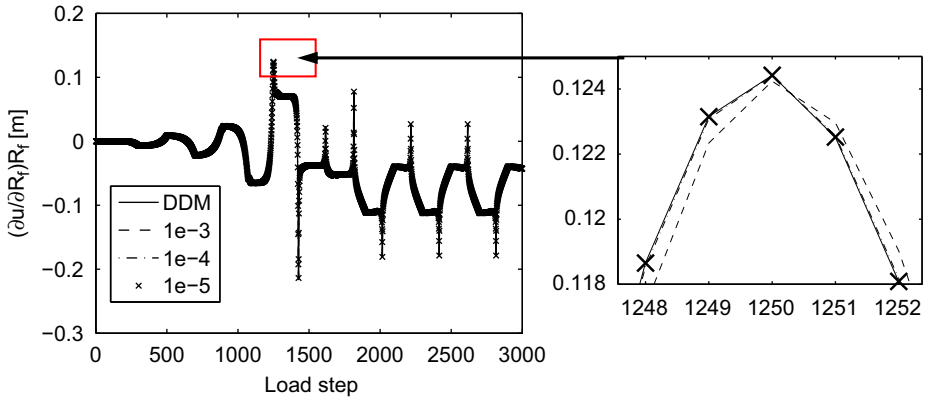

Fig. 7. Sensitivity of displacement of node A to R_f using DDM vs. FFD with different perturbation levels

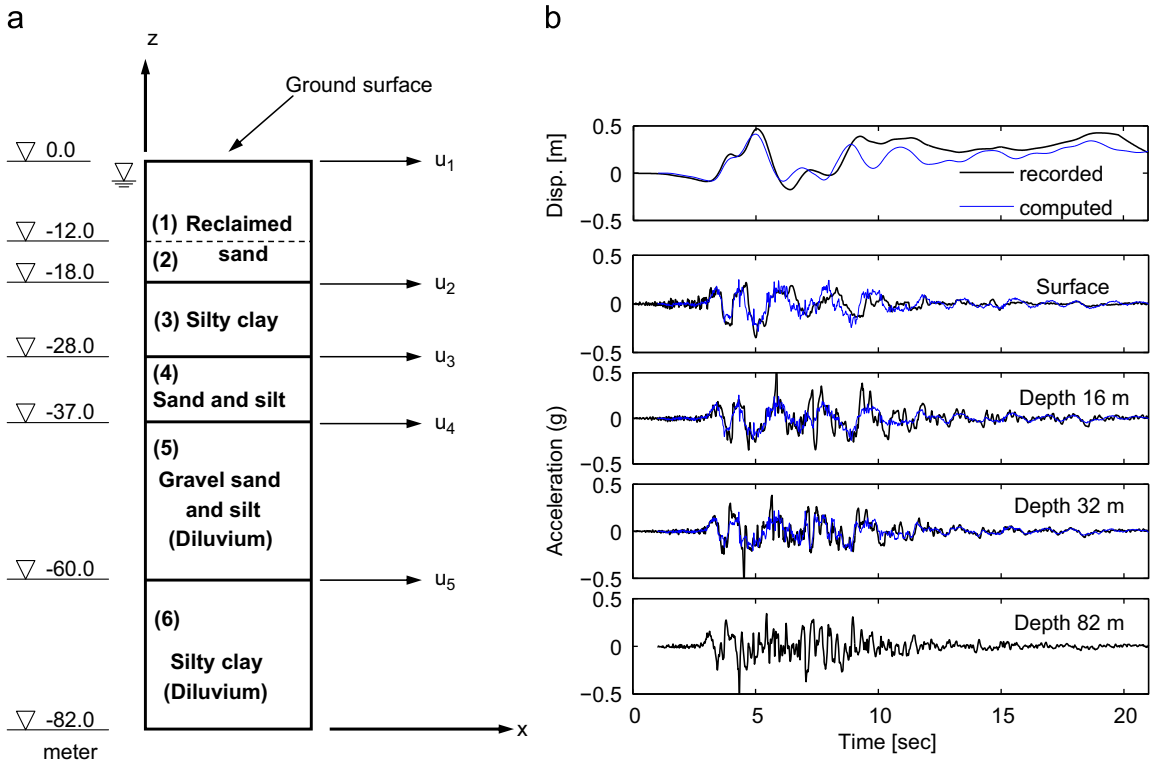

Fig. 8. (a) Soil profile of site at Port Island and (b) displacement history at ground surface and acceleration histories at various depths.

Table 1
Material parameters used in the example 2.

Materials	ρ (kg/m^3)	G_0	e_{in}	ν	R_f	d	k_r	h_r	γ	λ	ξ
1	2100	256	0.74	0.15	0.69	1.25	0.05	0.256	0.94	0.019	0.7
2	2100	232	0.53	0.15	0.67	1.25	0.05	0.345	0.94	0.019	0.7
3	1550	223	–	0.15	0.69	100	1	0.763	0.94	0.042	0.7
4	1950	317	0.76	0.17	0.89	5	0.5	0.243	0.94	0.019	0.7
5	2000	370	0.72	0.01	0.89	5	0.5	0.294	0.94	0.019	0.7
6	1750	374	–	0.27	0.69	100	1	0.757	0.94	0.025	0.7

Note: Parameters $a=0$, $b=2$, $m=3.6$, $n=0.75$ are used for all materials.

within the soil column. The actual acceleration recorded using the downhole array at a depth of 82 m is applied to the base of the FE model, see Fig. 8 (b). The Newmark-beta integration method is used with parameters $\alpha=0.55$ and $\beta=0.2756$ and a constant time step $\Delta t=0.01$ s. Good agreement is obtained between the recorded and computed horizontal displacement histories at the ground surface and between the recorded and computed acceleration histories at various soil depths, as can be seen in Fig. 8(b). A typical shear stress vs. shear strain response and a typical shear stress vs. effective confining pressure response in the top soil layer at a depth of 3.2 m are shown in Fig. 9. During shaking, excessive pore-pressure builds up progressively in the reclaimed sand, resulting in reduced effective confining pressure. Liquefaction in the top soil layer occurs at about 10 s, as is

Author's personal copy

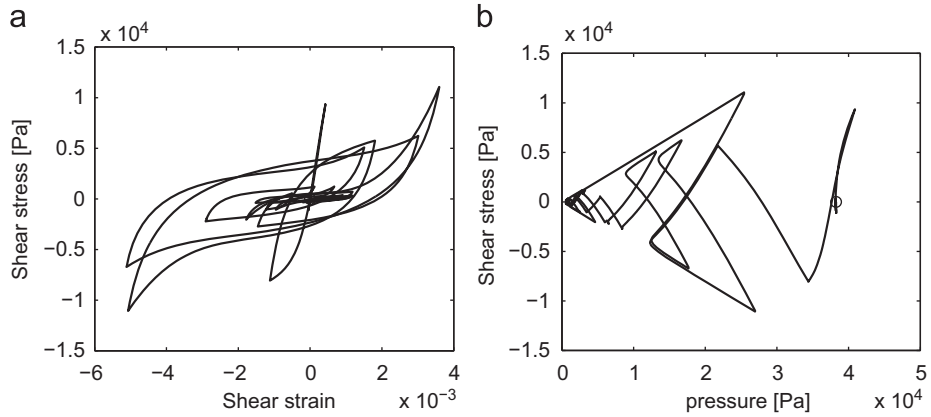

Fig. 9. (a) Shear stress vs. strain responses and (b) shear stress vs. mean effective pressure response in top soil layer at a depth of 3.2 m.

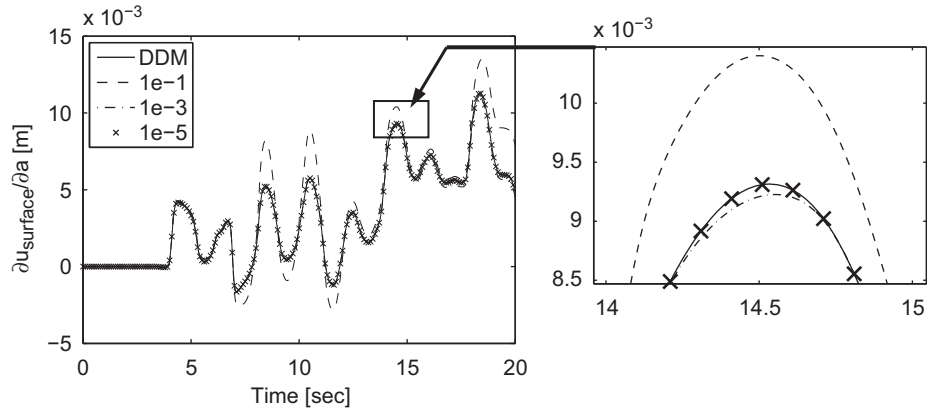

Fig. 10. Sensitivity of ground surface displacement to parameter a obtained using DDM vs FFD with different levels of parameter perturbation

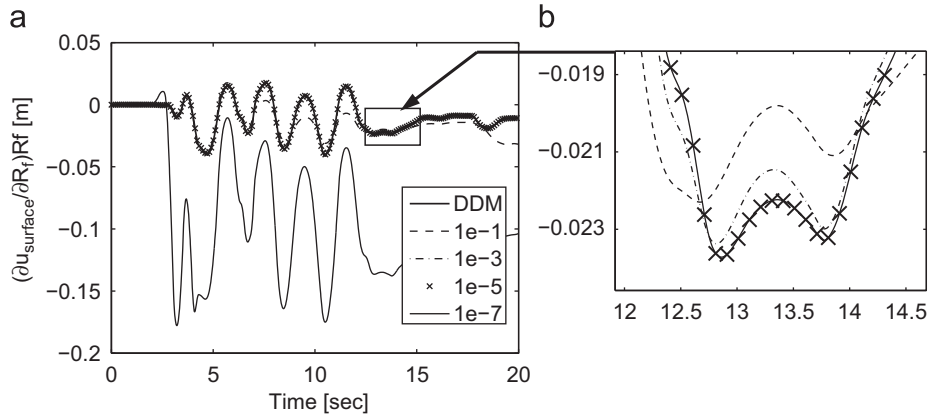

Fig. 11. Sensitivity of ground surface displacement to parameter R_f obtained using DDM vs. FFD with different levels of parameter perturbation

evidenced by the significant loss of strength and stiffness of the soil material. These figures demonstrate that the numerical simulation agrees well with the real recorded data, and the presented bounding surface model is able to capture the key features of the sand behavior including earthquake-induced liquefaction.

For practical interests, the sensitivity of the ground surface response to various material parameters of the top soil layer (i.e., layer #1 in Fig. 8(a)) is investigated. The DDM-based response sensitivity results are verified using the FFD method with different levels of parameter perturbation and are shown in Figs. 10–12. The FFD results are shown to converge asymptotically to the DDM results as the FFD perturbation reduces from 10^{-1} to $10^{-3}$and then 10^{-5}. Thus the DDM-based sensitivity algorithm and its implementation are verified to be correct for this multilayer soil system.

The advantage of the DDM method over the FFD method is evident from the following error analysis. If the round-off error of $\mathbf{u}$ from FE analysis is δ, then the error of parameter sensitivity $\frac{\partial \mathbf{u}}{\partial \theta}\theta$ from the DDM method is also in the order of δ. However, the error from the FFD method consists of two parts: the round-off errors in the order of $O(\frac{\theta}{\Delta\theta}\delta)$ where O is the Landau symbol; and the truncation error due to finite difference approximation is in the order of $O(\frac{\Delta\theta}{\theta})M$, where $M=\theta^2\cdot\frac{\partial^2 u}{\partial\theta^2}(\xi)$ is a finite number, $\xi\in[\theta,\theta+\Delta\theta]$.

Author's personal copy

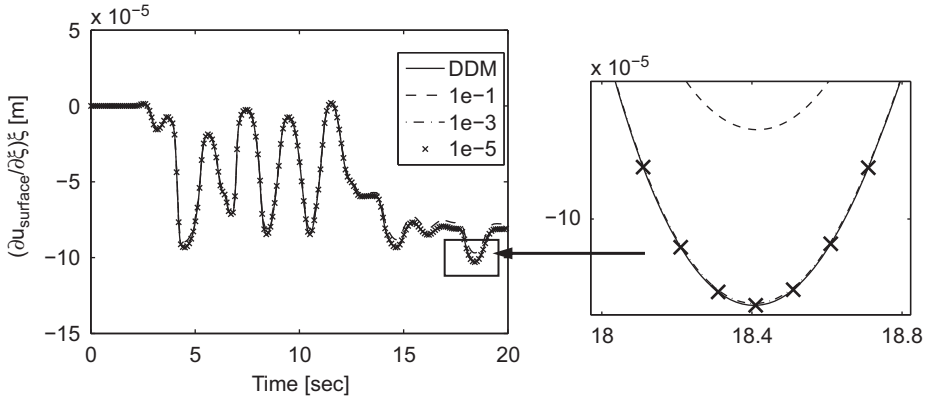

Fig. 12. Sensitivity of ground surface displacement to parameter ξ obtained using DDM vs. FFD with different levels of parameter perturbation

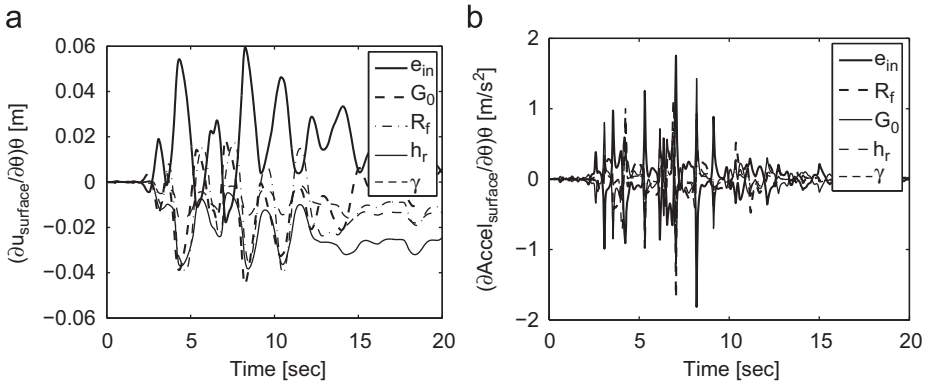

Fig. 13. (a) Relative importance of soil material parameters in regards to the horizontal displacement of the ground surface and (b) relative importance of soil material parameters in regards to the horizontal acceleration of the ground surface.

When $\Delta\theta/\theta$ is large, the truncation error term dominates, and so the total error from the FFD method decreases as $\Delta\theta/\theta$ is reduced. On the other hand, when $\Delta\theta/\theta$ is small enough, the round-off error $O(\frac{\theta}{\Delta\theta}\delta)$ becomes dominant. In this case, reducing $\Delta\theta/\theta$ continuously will induce large round-off errors in the FFD results. The significant limitation of the FFD method is illustrated in Fig. 11, where the FFD result is affected by the round-off errors and diverges significantly from the DDM results when $\Delta\theta/\theta = 10^{-7}$. In this example, the incremental displacement is used as the convergence criterion, which is set to be 10^{-12} m for verification purpose. However, the convergence criterion for the geotechnical systems is not necessarily so tight. In that case, it will be difficult to get accurate derivative using FFD method, and DDM becomes particularly useful.

The relative importance of system parameters in regard to the system response can be quantified according to the peak absolute value of the normalized response sensitivity time history $\frac{\partial \mathbf{u}}{\partial \theta}\theta$. Fig. 13(a) shows the normalized sensitivities of the horizontal displacement response of the ground surface to the five most sensitive material parameters of the top soil layer. The order of importance of these parameters (in descending order) is as follows: (1) the initial void ratio e_{in}, (2) the model constant G_0, (3) the failure deviatoric stress ratio R_f, (4) the constant parameter h_r for the plastic shear modulus, and (5) the constant parameter γ for the critical state line. The void ratio e_{in} is identified as the most important parameter affecting the ground surface displacement response. From Fig. 13(a), one can see that most parts of the sensitivity histories $\frac{\partial u_{surface}}{\partial e_{in}} e_{in}$ are positive. Thus, reducing the void ratio will reduce the ground surface displacement. Fig. 13(b) shows the normalized sensitivities of the horizontal acceleration response of the ground surface to the five most sensitive parameters of the top soil. These results indicate that the ground surface acceleration is most sensitive to the same set of parameters as the ground surface displacement, except that the order of importance is slightly changed (in descending order) to (1) e_{in}, (2) R_f, (3) G_0, (4) h_r, and (5) γ. From these observations, it is clear that the initial void ratio e_{in} is the controlling parameter affecting significantly both ground surface displacement and acceleration during earthquake excitation.

5. Conclusions

The DDM method is a general, accurate and efficient method for computing FE response sensitivities to model parameters, especially in the case of nonlinear materials. This paper applies the DDM-based response sensitivity analysis methodology to a bounding surface plasticity material model that has been widely used to simulate nonlinear sandy soil behaviors under static and dynamic loading conditions. The algorithm is implemented in the general-purpose nonlinear FE analysis software Open Sees. The new algorithm and its software implementation are validated through two application examples, in which the DDM-based response sensitivities are compared with their counterparts obtained using FFD analysis. The advantage of the DDM method over the FFD method is also highlighted through convergence tests.

In the application example, the normalized response sensitivity analysis results are also used to measure the relative importance of the soil constitutive parameters in regards to the ground surface displacement and acceleration in the case of ground liquefaction. The example illustrates the use of finite element

Author's personal copy

response sensitivity analysis to determine the relative importance of material parameters for specified system response parameters.

The work presented in this paper significantly broadens the application of DDM-based response sensitivity analysis, since it enables numerous applications involving the use of the bounding surface plasticity material model. Work is underway to extend the present study to sensitivity analysis of large-scale nonlinear soil-structure interaction systems.

Acknowledgments

Quan Gu acknowledges the financial support provided to him by the Fundamental Research Funds for the Central Universities of China (award no. 2010111075). Gang Wang would like to thank the financial support from Research Project Competition (UGC/HKUST) grant No. RPC11EG27 and Hong Kong Research Grants Council (RGC) grant No. 620311. Any opinions, findings, conclusions, or recommendations expressed in this publication are those of the authors and do not necessarily reflect the views of the sponsors.

References

[1] Kleiber M, Antunez H, Hien TD, Kowalczyk V. Parameter sensitivity in nonlinear mechanics: theory and finite element computations. Wiley; 1997.
[2] Conte JP, Vijalapura PK, Meghella M. Consistent finite element response sensitivity analysis. Journal of Engineering Mechanics 2003;129(12):1380–93.
[3] Barbato M, Gu Q. Probabilistic pushover analysis of structural and geotechnical systems. Journal of Structural Engineering 2010;136(11):1330–41.
[4] Ditlevsen O, Madsen HO. Structural reliability methods. Wiley; 1996.
[5] Gu Q, Conte JP, Elgamal A, Yang Z. Finite element response sensitivity analysis of multi-yield-surface J2 plasticity model by direct differentiation method. Computer Methods in Applied Mechanics and Engineering 2009;198(30–32):2272–85.
[6] Zhang Y, Der Kiureghian A. Dynamic response sensitivity of inelastic structures. Computer Methods in Applied Mechanics and Engineering 1993;108:23–36.
[7] Conte JP. Finite element response sensitivity analysis in earthquake engineering. Earthquake Engineering Frontiers in the New Millennium. In: Spencer, Hu, editors. Swets and Zeitlinger; 2001 395-401.
[8] Conte JP, Barbato M, Spacone E. Finite element response sensitivity analysis using force-based frame models. International Journal of Numerical Methods in Engineering 2004;59(13):1781–820.
[9] Gu Q, Barbato M, Conte JP. Handling of constraints in finite element response sensitivity analysis. Journal of Engineering Mechanics 2009;135(12):1427–38.
[10] Scott MH, Franchin P, Fenves GL, Filippou FC. Response sensitivity for nonlinear beam-column elements. Journal of Structural Engineering 2004;130(9):1281–8.
[11] Haukaas T, Der Kiureghian A. Strategies for finding the design point in nonlinear finite element reliability analysis. Journal of Probabilistic Engineering Mechanics 2006;21(2):133–47.
[12] McKenna F, Fenves GL. The OpenSees command language manual, Version 1.2. Pacific Earthquake Engineering Research Center, University of California at Berkeley; 2001, 〈http://opensees.berkeley.edu〉.
[13] Gu Q, Barbato M, Conte JP, Li Y. OpenSees command language manual—Response sensitivity analysis based on the direct differentiation method (DDM); 2010, 〈http://opensees.berkeley.edu/wiki/index.php/Sensitivity_Analysis〉.
[14] Der Kiureghian A, Haukaas T, Fujimura K. Structural reliability software at the University of California, Berkeley. Structural Safety 2006;28:44–67.
[15] Haukaas T, Der Kiureghian A. Methods and object-oriented software for FE reliability and sensitivity analysis with application to a bridge structure. Journal of Computing in Civil Engineering 2007;21(3):151–63.
[16] Scott MH, Haukaas T. Software framework for parameter updating and finite element response sensitivity analysis. Journal of Computing in Civil Engineering 2008;22(5):281–91.
[17] Gu Q. Finite element response sensitivity and reliability analysis of soil-foundation-structure-interaction systems. PhD Dissertation. Department of Structural Engineering, University of California, San Diego; 2008.
[18] Dafalias YF. Bounding surface plasticity. I: Mathematical foundation and hypoplasticity. Journal of Engineering Mechanics 1986;112(9):966–87.
[19] Wang ZL, Dafalias YF. Bounding surface hypoplasticity model for sand. Journal of Engineering Mechanics 1990;116(5):983–1002.
[20] Li XS, Dafalias YF, Wang ZL. State dependent dilatancy in critical state constitutive modeling of sand. Canadian Geotechnical Journal 1999;36(4):559–611.
[21] Li XSA. sand model with state-dependent dilatancy. Géotechnique 2002;52(3):173–86.
[22] Wang ZL, Makdisi FI, Egan J. Practical applications of a nonlinear approach to analysis of earthquake-induced liquefaction and deformation of earth structures. Soil Dynamics and Earthquake Engineering 2006;26(2–4):231–52.
[23] Richart FE, Hall JR, Woods RD. Vibrations of soils and foundations. Englewood Cliffs, N.J: Prentice-Hall, Inc.; 1970.
[24] Barbato M, Zona A, Conte JP. Finite element response sensitivity analysis using three-field mixed formulation: general theory and application to frame structures. International Journal for Numerical Methods in Engineering 2007;69(1):114–61.
[25] Chopra AK. Dynamics of structures: Theory and applications to earthquake engineering. Third Edition New Jersey: Prentice Hall; 2007.
[26] Simo JC, TJR Hughes. Computational inelasticity. New York: Springer-Verlag; 1998.
[27] Vidal CA, Lee HS, Haber RB. The consistent tangent operator for design sensitivity analysis of history-dependent response. Computer Systems in Engineering 1991;2(5–6):509–23.
[28] Zienkiewicz OC, Chan AHC, Pastor M, Schrefler BA, Shiomi T. Computational geomechanics with special reference to earthquake engineering. First EditionWiley; 1999.
[29] Elgamal A, Zeghal M, Parra E. Liquefaction of reclaimed island in Kobe, Japan. Journal of Geotechnical Engineering 1996;122(1):39–49.
[30] Arulanandan K, Li XS, Siva K. Numerical simulation of liquefaction-induced deformations. Journal of Geotechnical and Geoenvironmental Engineering 2000;126(7):657–66.